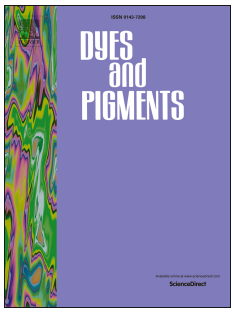

Syntheses, kinetics and thermodynamics of BODIPY-based fluorescent probes with different kinds of hydrophilic groups for the detection of biothiols

Lian-Xun Gao, Ming Tian, Lu Zhang, Yi Liu, Feng-Lei Jiang

PII: S0143-7208(20)30744-0

DOI: https://doi.org/10.1016/j.dyepig.2020.108434

Reference: DYPI 108434

To appear in: *Dyes and Pigments*

Received Date: 23 March 2020

Revised Date: 2 April 2020

Accepted Date: 5 April 2020

Please cite this article as: Gao L-X, Tian M, Zhang L, Liu Y, Jiang F-L, Syntheses, kinetics and thermodynamics of BODIPY-based fluorescent probes with different kinds of hydrophilic groups for the detection of biothiols, *Dyes and Pigments* (2020), doi: https://doi.org/10.1016/j.dyepig.2020.108434.

Author Statement

Lian-Xun Gao: Methodology, Investigation, Formal analysis, Writing - original draft. Ming Tian: Methodology, Investigation. Lu Zhang: Investigation. Yi Liu: Resources, Supervision, Funding acquisition. Feng-Lei Jiang: Supervision, Writing - review & editing, Funding acquisition.

Table of contents

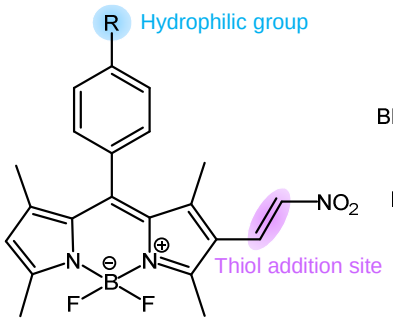

BDP: R = H

BDP-OEG: R = $O(CH_2CH_2O)_3CH_3$

BDP-OH: R = OH

BDP-QA: R = $\overset{\oplus}{N}(CH_3)_3$

Syntheses, kinetics and thermodynamics of BODIPY-based fluorescent probes with different kinds of hydrophilic groups for the detection of biothiols

Lian-Xun Gao,[a] Ming Tian, [a] Lu Zhang, [a] Yi Liu [a,b,c] and Feng-Lei Jiang [a,*]

[a] Sauvage Center for Molecular Sciences, College of Chemistry and Molecular Sciences, Wuhan University, Wuhan 430072, P. R. China.

[b] Hubei Province Key Laboratory for Coal Conversion and New Carbon Materials, School of Chemistry and Chemical Engineering, Wuhan University of Science and Technology, Wuhan 430081, P. R. China

[c] Guangxi Key Laboratory of Natural Polymer Chemistry, College of Chemistry and Materials Science, Nanning Normal University, Nanning 530001, P. R. China

[*] Corresponding author. Email: fljiang@whu.edu.cn (F.-L. Jiang)

Abstract

A series of BODIPY-based fluorescent probes incorporating different kinds of hydrophilic groups were synthesized for the detection of biothiols (GSH as a representative target), namely **BDP** (control), **BDP-OH** (acidic), **BDP-OEG** (neutral and hydrophilic) and **BDP-QA** (cationic). The incorporation of nitroolefin unit (-CH=CH-NO_2) to the BODIPY core enabled the OFF-ON fluorescent probes. The results indicated that the absorption and fluorescence emission spectra of the probes were essentially not affected by the hydrophilic groups attached on the *para* position of the *meso* phenyl group. The reaction rate constants were affected by the hydrophilicity of probes. It was highly worth noting that the cationic **BDP-QA** had the fastest response toward biothiols owing to the best water solubility and the possible formation of ion pairs with thiolate ($R\text{-}S^-$). Thermodynamics illustrated that the reactions of probes with GSH all had negative enthalpy changes and negative entropy changes. Moreover, **BDP-QA** had the highest affinity toward GSH (K = 2.54 × 10^4 M^{-1}) and the smallest LOD value (182 nM), which benefited from its best water solubility. This work has primarily elucidated the effects of hydrophilic groups from the kinetic and thermodynamic perspectives. It will promote better design of fluorescent probes with fast response and high affinity.

Key words: fluorescent probe; water solubility; hydrophilic group; kinetics; thermodynamics

1. Introduction

Biothiols, including cysteine (Cys, 30 ~ 200 μM), homocysteine (Hcy, 5 ~ 15 μM) and glutathione (GSH, γ-glutamyl-cysteinyl-glycin, 1 ~ 10 mM), play crucial roles for the maintenance of cellular redox status and healthy operations of life systems [1-4]. GSH, the most abundant biothiol and a non-protein thiol in living cells, is regarded as a detoxifying antioxidant that protects cells against damage caused by harmful heavy metals, peroxides and free radicals and so on [5]. So, it is highly necessary to monitor and detect GSH level in living cells and tissues. In the past few decades, there were many methods to detect biothiols, such as electrochemical detection [6], high performance liquid chromatography (HPLC) [7], electrospray ionization mass spectrometry [8] and so on. Although these methods could realize the detection of biothiols, they have suffered from some drawbacks, such as complicated preparations and operations, expensive testing facilities and restricted applications in living cells [9]. It was worth noting that fluorescent probes attracted growing interest owing to their excellent properties, such as simple operation, low detection limit, applicability in living cells and tissues, *etc* [10-13]. Over the last decades, researchers have exploited plentiful fluorescent probes based on different fluorophores, such as rhodamine [14-16], coumarin [17-20], cyanine [21,22], BODIPY (boron-dipyrromethene) derivatives [23-28], *etc*. Among them, BODIPY fluorophores have advantages such as facile syntheses, structural versatility, tunable spectroscopic properties and high quantum yields [29]. Thus, it is a good choice for BODIPY probes to detect and monitor thiols in cells and tissues.

However, BODIPY fluorophores have some drawbacks: (□) poor water solubility [30], (□) slow response [28,31], and (□) intense fluorescent background [31]. These problems seriously impeded the applications of fluorescent probes in living cells. Therefore, many researchers have made an enormous number of achievements in the past decades. To resolve the water solubility of probes, researchers have employed many methods including introduction of ionic hydrophilic groups (anionic [32,33] and cationic [34,35]), neutral hydrophilic groups (polyethylene ethanol or polyether chain)

[36-39], water-soluble polypeptide [40-42], saccharides [43], amine [44] and amphiphilic groups [45], *etc*. These methods improved water solubility of probes and raised dispersion coefficients of probes by introducing hydrophilic groups. So the collision probability of reactant molecules would increase and the response could be faster according to collision theory. Though these achievements have been made, it is still unclear how the different hydrophilic groups affect the efficacies of BODIPY-based fluorescent probes. To address this challenge, we focused on the effects of hydrophilic groups on the reaction kinetics and thermodynamics. Obviously, we did not mean to develop an excellent fluorescent probe with high sensitivity and selectivity in this work. However, this mechanism study could promote better design of fluorescent probes with fast response and high affinity.

Because sulfydryl group (-SH) has strong nucleophilicity and coordination capability, many sensing mechanisms have been exploited to detect the biothiols, including cleavage of sulphonamide [46,47], sulfonate ester [48], Se-N bond cleavage [49], aryl substitution reactions [3], disulfide bond cleavage and cyclization [50,51], and Michael additions [52,53]. Many strategies have employed the Michael addition-based thiol sensing protocols [54-58]. In this work, the incorporation of nitroolefin unit (-CH=CH-NO_2) to the parent BODIPY dye would introduce a strong Micheal acceptor (Scheme 1), which would be highly susceptible to sulfhydryl nucleophiles [59,60]. Besides, the nitroolefin unit can improve the response rates of probes toward biothiols. When biothiols were reacted with nitroolefin by Michael addition, the photo-induced electron transfer (PET) and intramolecular charge transfer (ICT) were blocked and thereby the fluorescence of probes was switched on [31]. The effects of different hydrophilic groups (the R group in Scheme 1) were investigated on the sensing efficacies for *in vitro* biothiols from the kinetic and thermodynamic perspectives. Since we had already demonstrated the fluorescent imaging of intracellular biothiols with probes of similar structures in our previous work [28,31], we were convinced these probes can be applied in cell imaging as well.

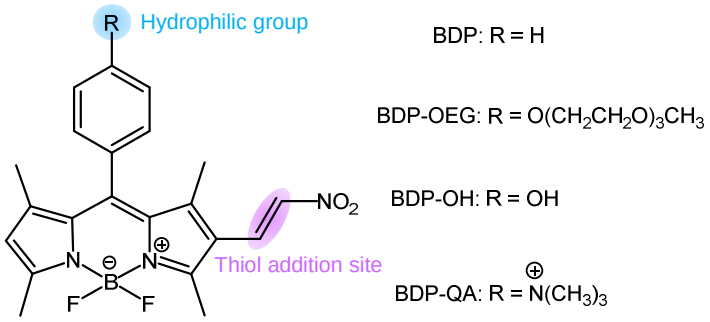

Scheme 1. The structures of the BODIPY-based fluorescent probes. The R group is modified for water solubility. The nitroolefin unit (-CH=CH-NO_2) is designed for sensing biothiols.

2. Experimental

2.1 Apparatus and reagents

The NMR spectra were measured in appropriate deuterated solvents on a Bruker AVANCE III HD 400 MHz spectrometer, using tetramethylsilane (TMS) as the internal standard. The electrospray ionization mass spectra (ESI-MS) were measured on an Agilent Q-TOF high resolution liquid chromatography mass spectrometer. The fluorescence spectra were measured by a LS-55 fluorescence spectrometer (PerkinElmer). Absolute quantum yields were determined by a FLS1000 fluorescence spectrometer with an integrating sphere (Edinburgh Instruments). The absorption spectra were measured by an Agilent Cary 100 UV-Vis double-beam spectrophotometer. All reagents and chemicals, unless stated otherwise, were purchased from commercial suppliers and used without further purification. Solvents were dried and distilled by drying agents under an inert atmosphere prior to use. Twice-distilled water was used throughout all experiments. The stock solution of probes was prepared at 1 mM in dimethylsulfoxide (DMSO). Testing solutions were prepared in 4-(2-hydroxyethyl)-1-piperazineethanesulfonic acid (HEPES) buffer solution (20 mM, pH = 7.4).

2.2 Syntheses of probes

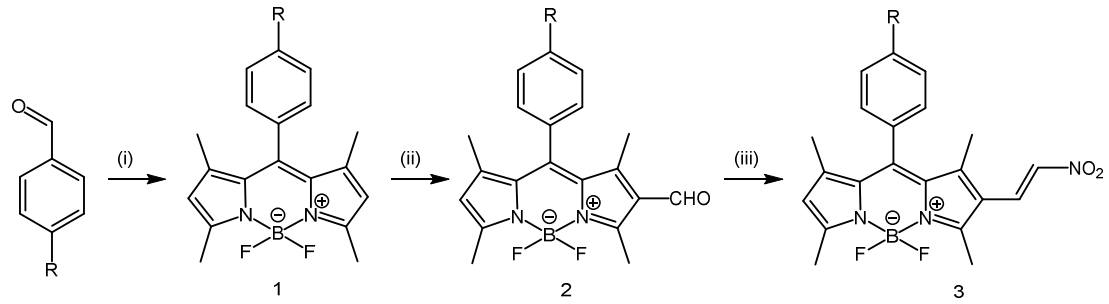

Scheme 2. Synthetic routes for **BDP**, **BDP-OEG**, **BDP-OH** and **3d**. (i) 2, 4-dimethyl-1H-pyrrole, TFA, DDQ, Et_3N, $BF_3.OEt_2$, DCM; (ii) phosphorus oxychloride, DMF, DCE, 62 □; (iii) piperidine, acetic acid glacial, CH_3NO_2, toluene.

2.2.1 Synthesis of 1a

Trifluoroacetic acid (TFA) (150 μL) was added to a solution of benzaldehyde (425 mg, 4 mmol) and 2,4-dimethylpyrrole (827 μL, 8 mmol) in 100 mL dichloromethane (DCM) under argon atmosphere. The reaction mixture was stirred at room temperature for 5 h. Then 2,3-dichloro-5,6-dicyano-1,4-benzoquinone (DDQ) (0.908 g, 4 mmol) was added to the mixture and stirred for 15 min. Triethylamine (Et_3N) (6.4 mL) was added dropwise to the reaction mixture and stirred for 15 min. Finally, $BF_3.OEt_2$ (7.0 mL) was added dropwise to the reaction mixture. The mixture was stirred at room temperature for 12 h. The resulting solution was extracted with water (2 × 200mL). The organic phase was dried over anhydrous Na_2SO_4. After removing the solvent in vacuum, the residue was purified by flash column chromatography on silica gel using DCM as the eluent. **1a** was obtained as a red solid (400 mg, yield: 31 %). ^{1}H NMR (400 MHz, $CDCl_3$): δ = 7.48 (t, 3H, J = 4.0 Hz), 7.29 - 7.26 (m, 2H), 5.98 (s, 2H), 2.56 (s, 6H), 1.37 (s, 6H). ^{13}C NMR (100 MHz, $CDCl_3$) δ = 155.44, 143.19, 141.75, 135.01, 131.45, 129.17, 128.96, 127.95, 121.22, 14.67, 14.65, 14.62, 14.40. ESI-MS: *m/z* calcd for $C_{19}H_{19}BF_2N_2$ $[M + H]^+$: 325.1682; found 325.1685.

2.2.2 Synthesis of 2a

The *N*,*N*-dimethylformamide (DMF) (3.0 mL) was stirred with ice bath under argon. The $POCl_3$ (3.0 mL) was dropwise added into the DMF and stirred for 10 min.

Then the mixture was stirred at room temperature for 30 min. Then **1a** (200 mg, 0.62 mmol) dissolved in 1,2-dichloroethane (DCE) (30 mL) was added dropwise in the mixture. The resulting mixture was stirred at 62 □ for 3 h. The reaction solution was cooled to room temperature and slowly dropped into saturated $NaHCO_3$ solution (150 mL) with an iced bath. Then the mixture was stirred for 30 min and washed with water (100 mL). The combined organic phase was dried over anhydrous Na_2SO_4 and evaporated in vacuum. The residue was further purified with column chromatography (CH_2Cl_2/petroleum = 25 :1) to gain **2a** as a red solid (160 mg, yield: 73 %). ^{1}H NMR (400 MHz, $CDCl_3$): δ = 10.00 (s, 1H), 7.54 - 7.52 (t, 3H, *J* = 4.0 Hz), 7.29 - 7.26 (m, 2H), 6.15 (s, 1H), 2.82 (s, 3H), 2.62 (s, 3H), 1.65 (s, 3H), 1.42 (s, 3H). ^{13}C NMR (100 MHz, $CDCl_3$): δ = 186.00, 161.69, 156.54, 147.35, 143.59, 142.98, 142.96, 134.17, 129.59, 129.53, 127.71, 126.32, 124.06, 15.16, 14.90, 13.08, 11.61. ESI-MS: *m/z* calcd for $C_{20}H_{19}BF_2N_2O$ $[M + H]^+$: 353.1631; found 353.1626.

2.2.3 Synthesis of 3a (BDP)

2a (170 mg, 0.49 mmol) was dissolved in toluene under argon. Then nitromethane (262 μL, 4.9 mmol), piperidine (300 μL) and glacial acid (300 μL) were added successively into the mixture. The mixture was stirred under reflux for 2 h. Then the reaction mixture was cooled to room temperature. Then the solvent was removed in vacuum. The crude product was purified by column chromatography (CH_2Cl_2/petroleum = 1:1) to gain **3a** (**BDP**) as a red solid (67 mg, yield: 35 %). ^{1}H NMR (400 MHz, $CDCl_3$): δ = 8.03 (d, 1H, *J* = 12.0 Hz), 7.54 (t, 3H, *J* = 4.0 Hz), 7.34 (d, 1H, *J* = 12.0 Hz), 7.30 - 7.26 (m, 2H), 6.15 (s, 1H), 2.71 (s, 3H), 2.61 (s, 3H), 1.47 (s, 3H), 1.42 (s, 3H). ^{13}C NMR (100 MHz, $CDCl_3$): δ = 161.55, 154.19, 147.37, 142.72, 140.41, 134.58, 134.16, 130.92, 129.67, 129.56, 127.82, 124.05, 120.08, 15.15, 14.95, 13.98, 12.84. ESI-MS: *m/z* calcd for $C_{21}H_{20}BF_2N_3O_2$ $[M + H]^+$: 396.1689; found 396.1702.

Compounds **1b**, **2b** and **3b** (**BDP-OEG**) were synthesized in the same ways as **1a**, **2a** and **3a** (**BDP**).

2.2.4 Synthesis of 1b

1b was gained as an orange yellow solid (225 mg, yield: 12 %). ^{1}H NMR (400 MHz, $CDCl_3$): δ = 7.15 (d, 2H, *J* = 12.0 Hz), 7.01 (d, 2H, *J* = 8.0 Hz), 5.96 (s, 2H), 4.18 (t, 2H, *J* = 6.0 Hz), 3.90 (t, 2H, *J* = 4.0 Hz), 3.78 - 3.76 (m, 2H), 3.72 - 3.70 (m, 2H), 3.68 - 3.66 (m, 2H), 3.57 - 3.55 (m, 2H), 3.38 (s, 3H), 2.54 (s, 6H), 1.41 (s, 6H). ^{13}C NMR (100 MHz, $CDCl_3$): δ = 159.35, 155.25, 143.20, 141.83, 131.84, 129.15, 127.20, 121.11, 115.19, 71.95, 70.90, 70.69, 70.62, 69.76, 67.48, 59.12, 14.65; ESI-MS: *m/z* calcd for $C_{26}H_{33}BF_2N_2O_4$ $[M + H]^+$: 487.2574; found 487.2589.

2.2.5 Synthesis of 2b

2b was gained as a yellow solid (95 mg, yield: 58 %). ^{1}H NMR (400 MHz, $CDCl_3$): δ = 9.99 (s, 1H), 7.14 (d, 2H, *J* = 8.0 Hz), 7.04 (d, 2H, *J* = 8.0 Hz), 6.13 (s, 1H), 4.19 (t, 2H, *J* = 6.0 Hz), 3.90 (t, 2H, *J* = 6.0 Hz), 3.78 - 3.75 (m, 2H), 3.71 - 3.67 (m, 2H), 3.66 - 3.65 (m, 2H), 3.57 - 3.55 (m, 2H), 3.37 (s, 3H), 2.80 (s, 3H), 2.59 (s, 3H), 1.69 (s, 3H), 1.46 (s, 3H). ^{13}C NMR (100 MHz, $CDCl_3$): δ = 184.97, 165.65, 160.41, 158.73, 155.31, 146.35, 142.69, 141.85, 133.45, 129.14, 127.92, 125.20, 122.90, 114.48, 70.89, 69.86, 69.63, 69.56, 68.65, 66.51, 58.06, 14.13, 13.05, 12.01, 10.80; ESI-MS: *m/z* calcd for $C_{27}H_{33}BF_2N_2O_5$ $[M + H]^+$: 515.2523; found 515.2537.

2.2.6 Synthesis of 3b (BDP-OEG)

3b (**BDP-OEG**) was gained a yellow solid (25 mg, yield: 25 %). ^{1}H NMR (400 MHz, $CDCl_3$): δ = 8.01 (d, 1H, *J* = 16.0 Hz), 7.33 (d, 1H, *J* = 12 Hz), 7.14 (d, 2H, *J* = 8.0 Hz), 7.05 (d, 2H, *J* = 8.0 Hz), 6.13 (s, 1H), 4.19(t, 2H, *J* = 4.0 Hz), 3.91 (t, 2H, *J* = 4.0 Hz), 3.77 (t, 2H, J = 4 Hz), 3.71 - 3.69 (m, 2H), 3.67 - 3.65 (m, 2H), 3.57 - 3.55 (m, 2H), 3.38 (s, 3H), 2.68 (s, 3H), 2.58 (s, 3H), 1.51 (s, 3H), 1.45 (s, 3H). ^{13}C NMR (100 MHz, $CDCl_3$): δ = 161.35, 159.83, 154.03, 147.44, 142.86, 140.38, 134.46, 134.24, 131.11, 130.99, 129.20, 129.09, 126.20, 123.96, 119.99, 115.70, 115.56, 71.93, 70.90, 70.66, 70.59, 69.89, 67.56, 59.10, 15.23, 15.11, 13.94, 13.06; ESI-MS: *m/z* calcd for $C_{28}H_{34}BF_2N_3O_6$ $[M + H]^+$: 558.2581; found 558.2594.

Compound **3c** (**BDP-OH**) was synthesized according to the previous literature [31].

2.2.7 Synthesis of 3c (BDP-OH)

3c (**BDP-OH**) was gained as a dark red solid (45 mg, yield: 34 % with step iii in Scheme 2). ^{1}H NMR (400 MHz, $CDCl_3$): δ = 8.05 (d, 1H, J = 16.0 Hz), 7.36 (d, 1H, J = 16.0 Hz), 7.13 (d, 2H, J = 8.0 Hz), 7.02 (d, 2H, J = 8.0 Hz), 6.16 (s, 1H), 2.71 (s, 3H), 2.62 (s, 3H), 1.51 (s, 3H), 1.26 (s, 3H). ^{13}C NMR (100 MHz, $CDCl_3$): δ = 160.35, 156.04, 153.04, 146.39, 141.84, 139.33, 133.39, 133.23, 133.23, 130.07, 128.26, 124.98, 122.96, 122.94, 118.95, 118.93, 115.52, 14.17, 14.09, 12.91, 12.01; ESI-MS: *m/z* calcd for $C_{21}H_{20}BF_2N_3O_3$ $[M - H]^-$: 410.1493; found 410.1498.

Compounds **1d**, **2d** and **3d** were synthesized in same ways as **1a**, **2a** and **3a** (**BDP**).

2.2.8 Synthesis of 1d

1d was gained as a red solid (300 mg, yield: 21 %). ^{1}H NMR (400 MHz, $CDCl_3$): δ = 7.06 (d, 2H, J = 12.0 Hz), 6.77 (d, 2H, J = 12.0 Hz), 5.97 (s, 2H), 3.02 (s, 6H), 2.55 (s, 6H), 1.48 (s, 6H). ^{13}C NMR (100 MHz, $CDCl_3$): δ =154.73, 150.66, 143.29, 143.24, 132.21, 128.74, 122.16, 120.86, 112.34, 40.37, 14.75; ESI-MS: *m/z* calcd for $C_{21}H_{24}BF_2N_3$ $[M + H]^+$: 368.2104; found 368.2114.

2.2.9 Synthesis of 2d

2d was gained as a black solid (135 mg, yield: 61 %). ^{1}H NMR (400 MHz, $CDCl_3$): δ = 10.01 (s, 1H), 7.05 (d, 2H, J = 12.0 Hz), 6.79 (d, 2H, J = 8.0 Hz), 6.13 (s, 1H), 3.04 (s, 6H), 2.82 (s, 3H), 2.60 (s, 3H),1.77 (s, 3H),1.54 (s, 3H). ^{13}C NMR (100 MHz, $CDCl_3$): δ = 186.11, 160.71, 156.03, 156.01, 150.97, 147.46, 145.23, 142.95,128.63, 123.60, 123.58, 123.55, 120.99, 112.38, 112.31, 40.30, 15.32, 15.09, 13.03, 13.05, 12.00; ESI-MS: *m/z* calcd for $C_{22}H_{24}BF_2N_3O$ $[M + H]^+$: 396.2053; found 396.2065.

2.2.10 Synthesis of 3d

3d was gained as a dark red solid (74 mg, yield: 52 %). ^{1}H NMR (400 MHz, $CDCl_3$): δ = 8.05 (d, 1H, J = 12.0 Hz), 7.36 (d, 1H, J = 12.0 Hz), 7.05 (d, 2H, J = 8.0 Hz), 6.80 (d, 2H, J = 8.0 Hz), 6.14 (s, 1H), 3.05 (s, 6H), 2.70 (s, 3H), 2.60 (s, 3H), 1.69 (s, 3H), 1.54 (s, 3H). ^{13}C NMR (100 MHz, $CDCl_3$): δ = 160.68, 153.79, 150.95, 147.52, 144.34, 140.44, 134.24, 131.61, 131.28, 128.80, 123.66, 121.02, 119.89, 119.87, 119.83, 112.44, 40.35, 15.39, 15.09, 13.87, 13.28; ESI-MS: *m/z* calcd for $C_{23}H_{25}BF_2N_4O_2$ $[M + H]^+$: 439.2111; found 439.2121.

2.2.11 Synthesis of BDP-QA

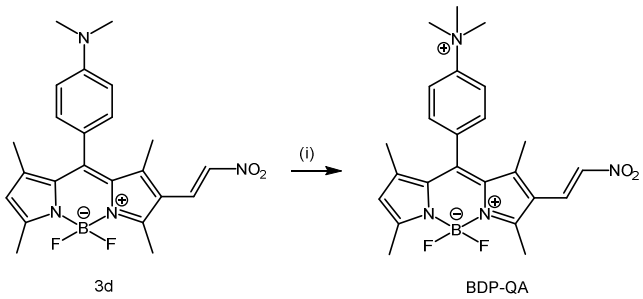

Scheme 3. Synthetic route for **BDP-QA**. (i) iodomethane, acetonitrile, argon, room temperature.

3d (57 mg, 0.13 mmol) was dissolved in acetonitrile under argon atmosphere. Iodomethane (828 μL, 13 mmol) was dropwise added into the solution. The reaction mixture was stirred at room temperature for 24 h. Then the solvent was removed in vacuum. The crude product was purified by column chromatography (methyl alcohol as eluent) to gain **BDP-QA** as a yellow solid (25 mg, yield: 42 %). ^{1}H NMR (400 MHz, DMSO): δ = 8.24 (d, 2H, J = 12.0 Hz), 7.97 (d, 1H, J = 12.0 Hz), 7.76 (d, 2H, J = 8.0 Hz), 7.60 (d, 1H, J = 12.0 Hz), 6.45 (s, 1H), 3.72 (s, 9H), 2.67 (s, 3H), 2.55 (s, 3H), 1.46 (s, 3H), 1.37 (s, 3H); ESI-MS: *m/z* calcd for $C_{24}H_{28}BF_2N_4O_2$ $[M]^+$: 453.2273; found 453.2279.

2.3 Kinetic and thermodynamic experiments

For kinetic parameters, the concentrations of Cys, Hcy and GSH were 100-fold of those of probes. So, the reactions of probes with biothiols could be regarded as pseudo-first-order kinetics. We added GSH into the HEPES buffer solution of probes and detected the fluorescence intensity as time by a fluorescence spectrometer at varied temperatures. For thermodynamic parameters, we conducted the titration experiments in HEPES buffer at varied temperatures.

3. Results and discussion

To investigate the effects of hydrophilic groups on the efficacies of probes, we chose BODIPY as the fluorophore and nitroolefin (-CH=CH-NO_2) as the sensing unit for biothiols (Scheme 1). We synthesized four probes conjugating different hydrophilic groups, namely **BDP** (control), **BDP-OH** (acidic), **BDP-OEG** (neutral and hydrophilic) and **BDP-QA** (cationic). The neutral **BDP** was synthesized as the control to study the properties of different substituents at the *para* position of phenyl group attached to the BODIPY core. The neutral (oligo ethylene glycol, -**OEG**), acidic (-**OH**) and quaternary ammonium (-**QA**) substituents at the *para* position of phenyl group endowed the BODIPY-based fluorescent probes water-solubility. All the compounds reported herein were carefully characterized by ^{1}H NMR, ^{13}C NMR and high resolution ESI mass spectrometry (Figs. S1 - 32 in the Supporting Information). The ^{13}C NMR data of **BDP-QA** was not available yet because its ^{13}C NMR signal was very weak. However, the ^{1}H NMR (Fig. S31) and HRMS (Fig. S32) characterization of **BDP-QA** can well confirm its chemical structure. The intracellular concentrations of Cys, Hcy and GSH were in the range of 30 ~ 200 μM, 5 ~ 15 μM, 1 ~ 10 mM, respectively. Since GSH was the predominant biothiol in cells, it was selected as the sensing target in this work.

First, we investigated whether the hydrophilic groups affected the optical properties of probes. The fluorescence and UV-Vis absorption spectra of probes were measured in HEPES buffer solutions containing ~ 1% DMSO brought by dilution from the stock solution (prepared in DMSO), *i.e.* almost 100% aqueous solutions. Most of the previous works conducted the sensing of biothiols in a mixture solution of water and organic solvents, acetonitrile (ACN) from example [5,11,28,31,61]. As shown in Fig. 1a, when **BDP-QA** was reacted with excess GSH in the HEPES buffer, the absorption maximum was slightly blue-shifted for 1 nm. Besides, the molar absorption coefficient slightly increased, presumably owing to the enhancement of dispersion coefficient of the adduct **BDP-QA**-GSH. The emission maximum of **BDP-QA** was red-shifted for 12 nm when reacted with GSH in the HEPES buffer, possibly due to the aggregation of BODIPY fluorophores in water. In contrast, the absorption and emission maxima were blue-shifted in DMSO for 19 and 25 nm (Table S1),

respectively, which was clearly resulted from the decrease of π-conjugation after the addition of GSH to **BDP-QA** (Fig. S33a). The solvent had obvious influence on the optical response of BODIPY probes. Compromises between the aggregation (red shift) and the decreased π-conjugation (blue shift) were present in the absorption and emission spectra when the probes were applied in the HEPES buffer. This can well explain the blue shift of only 1~4 nm in the absorption spectra of probes in the HEPES buffer after the conjugate addition with GSH. The optical properties of other probes were similar as that of **BDP-QA** (Table 1 and Figs. S33 - 36). The absorption and emission maxima of these four probes were all at 507 ± 1 nm and 512 ± 1 nm, respectively, obviously demonstrating that the substitution with hydrophilic groups on the *para* position of *meso*-phenyl group of BODIPY essentially did not affect the π-conjugation and the HOMO-LUMO gap. The low quantum yields (QYs) of these four fluorescent probes in the HEPES buffer were presumably caused by PET and ICT as well as aggregation-caused quenching (ACQ). After they were reacted with GSH, the quantum yields of adducts were obviously different, maybe due to their different water solubility. As shown in Fig. 1b, when **BDP-QA** was reacted with different small biological molecules with corresponding biological concentrations, fluorescent enhancement up to 28-fold was observed in the presence of 10 mM GSH, the concentration likewise in cells. In the cellular conditions, the fluorescent probes would mostly report the signal caused by GSH. **BDP**, **BDP-OH** and **BDP-OEG** had similar results (Figs. S34 - 36). These results indicated that all the probes could recognize GSH in the cellular conditions.

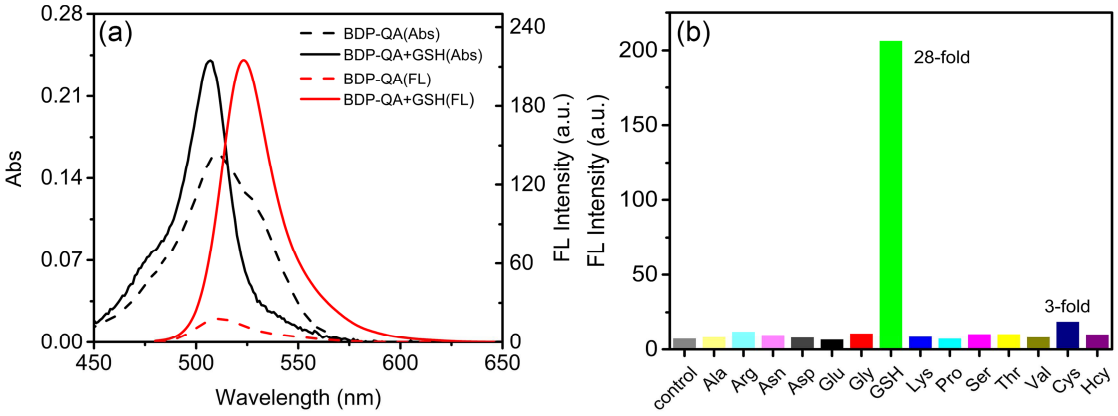

Fig. 1. The optical properties of **BDP-QA**. (a) The fluorescence and absorption spectra of **BDP-QA** in the HEPES buffer solution and (b) the selectivity of **BDP-QA** (10 μM). Except for Cys (200 μM), Hcy (15 μM) and GSH (10 mM), the concentration of other analytes was 1 mM respectively. The concentrations of Cys, Hcy and GSH are close to those in cellular conditions.

Table 1. Photophysical properties of probes in the absence and presence of GSH in the HEPES buffer solution. QY represents the absolute quantum yield.

	λ_{abs} (nm)	λ_{em} (nm)	QY (%)
BDP	506	510	< 0.01
BDP + GSH	505	516	3.97
BDP-OEG	507	513	< 0.01
BDP-OEG + GSH	503	518	4.57
BDP-OH	505	512	< 0.01
BDP-OH + GSH	503	517	1.64
BDP-QA	508	512	0.58
BDP-QA + GSH	507	524	15.21

Then, we explored whether hydrophilic groups affected the reaction rates of probes toward GSH. When the concentration of GSH was 100 times larger than that of a probe, the reaction can be regarded as pseudo-first-order kinetics. So, we can describe the dependence of the probe concentration (c) on the reaction time (t) by eq. (1):

$$c = c_0 \times \exp(-kt)$$

where c_0 represents the original concentration of probe (reactant), k is the reaction rate constant. When the probes were reacted with GSH, the PET and ICT processes would be blocked and thereafter the fluorescence of probes was switched on. So the enhancement of fluorescence intensity can be used to reflect the product concentration. The kinetics can be fitted by eq. (2):

$$I = \mathrm{a} \times \exp(kt) + \mathrm{b}$$

where a and b are constants without physical significance, *I* represents fluorescence intensity of the resulting product, *k* represents the rate constant, and *t* is the reaction time. As shown in Fig. 2a, when **BDP-QA** was reacted with Cys, Hcy and GSH at 298 K, their apparent rate constants were 0.102 s^{-1}, 0.0259 s^{-1} and 0.0162 s^{-1}, respectively. The results indicated that a biothiol of larger molecular weight had smaller rate constant. The reaction rate constants were affected by the steric hindrance of biothiols. Among the three biothiols, GSH (a tripeptide) had the largest molecular weight and therefore the largest steric hindrance as well as the smallest diffusion rate. So, the rate constant for GSH was the smallest. Besides, the half-time ($t_{1/2}$) of the pseudo-first-order reaction obeys the following eq. (3):

$$t_{1/2} = \frac{ln2}{k}$$

So the half-time $t_{1/2}$ of the reaction of **BDP-QA** with GSH was 43 s at 298 K. From Fig. 2b, as the temperature increased, the rate constants gradually increased owing to more vigorous molecular movement in the reaction system. However, the more vigorous collision would lead to strengthened non-radiative relaxation and therefore weakened fluorescence. The dependence of *k* on temperature *T* is simulated by the Arrhenius equation, eq. (4):

$$k = \mathrm{A} \times \exp\left(-\frac{E_a}{RT}\right)$$

where A is the pre-exponential factor that represents the frequency of collisions between reactive molecules, E_a represents the activation energy, and *R* is the gas constant (8.314 J mol^{-1} K^{-1}). As shown in Fig. 2c, the apparent activation energy (E_a) was 75.24 kJ mol^{-1} and pre-exponential factor (A) was 2.56×10^{11} s^{-1} for the reaction of **BDP-QA** with GSH. We also completed kinetic investigations for other probes (**BDP**, **BDP-OEG** and **BDP-OH**) (Table 2 and Figs. S37 - 39). The kinetic parameters were the mean of three independent experiments. **BDP-QA** had the largest rate constant. The activation energy had no obvious changes, so these probes should have the same reaction mechanism and hydrophilic groups had no obvious effect on it. The reactions of these probes with Hcy showed the similar trend (Table S2).

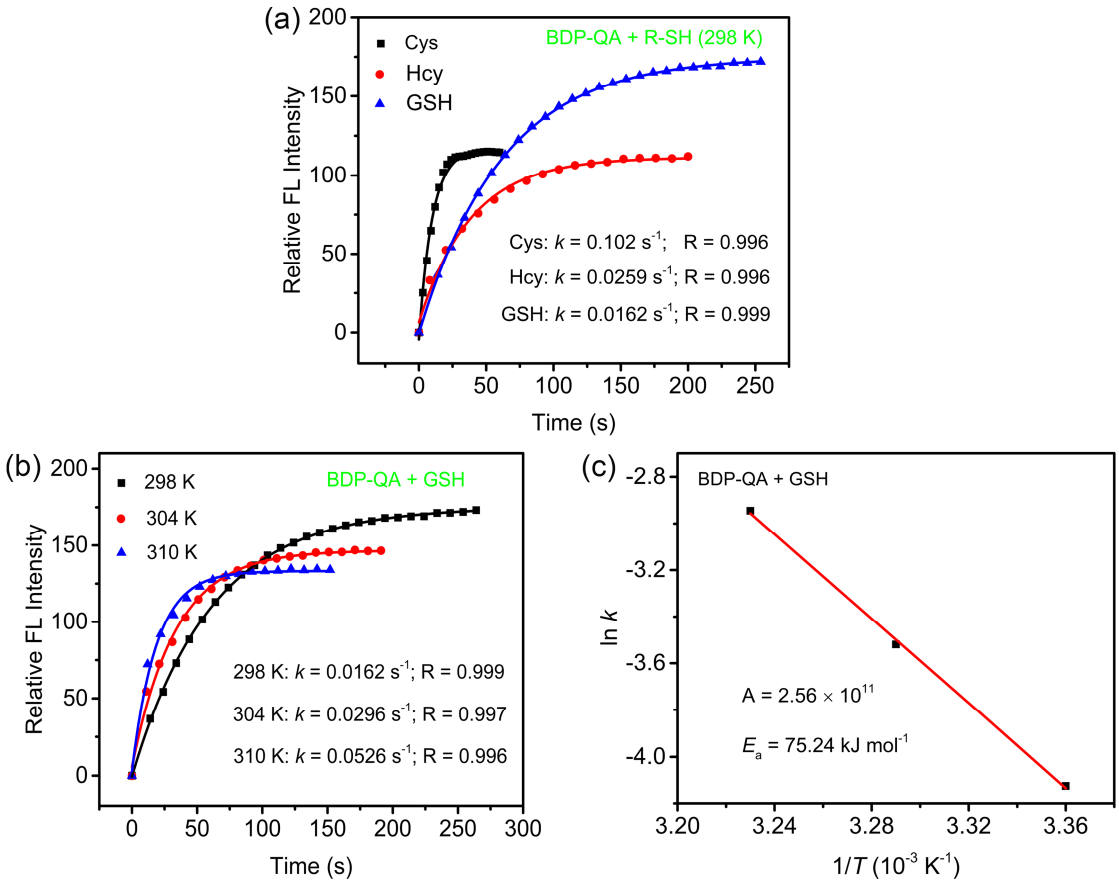

Fig. 2. Kinetics of **BDP-QA** (10 μM) and thiols (1 mM) in HEPES buffer. (a) The reactions of **BDP-QA** with Cys, Hcy and GSH at 298K; (b) The reactions of **BDP-QA** with GSH at different temperatures; (c) The relationship of ln *k* with 1/*T* for the reaction of **BDP-QA** with GSH.

Table 2. The kinetic parameters of probes reacted with GSH in the HEPES buffer. The data are the mean of three independent experiments.

Probes	k [a] (10^{-3} s^{-1})	$t_{1/2}$ [a, b] (s)	E_a (kJ mol^{-1})	lnA
BDP	3.06 ± 0.23	228 ± 18	73.49 ± 8.27	23.85 ± 3.26
BDO-OEG	3.94 ± 0.34	177 ± 16	59.84 ± 8.60	18.58 ± 3.29
BDP-OH	5.24 ± 0.73	133 ± 21	73.33 ± 8.27	23.27 ± 3.54
BDP-QA	18.53 ± 2.77	38 ± 6	69.92 ± 4.61	24.26 ± 1.74

[a] The reactions proceed at 298 K. [b] The half-time of pseudo-first-order reaction.

Next, we investigated the reaction mechanism of probes with biothiols, GSH for example. As shown in Scheme 4, speculative reaction mechanism of probes with biothiols was proposed according to the nucleophilic addition [62-64]. The nitro unit ($-NO_2$) was a very strong electron-withdrawing group (EWG), which could make the nucleophilic addition happen. First, GSH dissociated as GS^- and H^+ (Step 1). Then GS^- attacked the olefinic bond and formed the carbanion (Step 2), which should be the rate-determining step (RDS) for this reaction [62-64]. The conjugate addition would result in the turn-on fluorescence. Finally, protonation of the carbanion resulted in the addition product (Step 3). In the HEPES buffer with a pH of 7.4, there might be only a minor concentration of GS^-. Besides the above speculative mechanism, GSH can possibly attack the nitroolefin and then proton transfer occurred from the intermediate since the -SH group was highly nucleophilic.

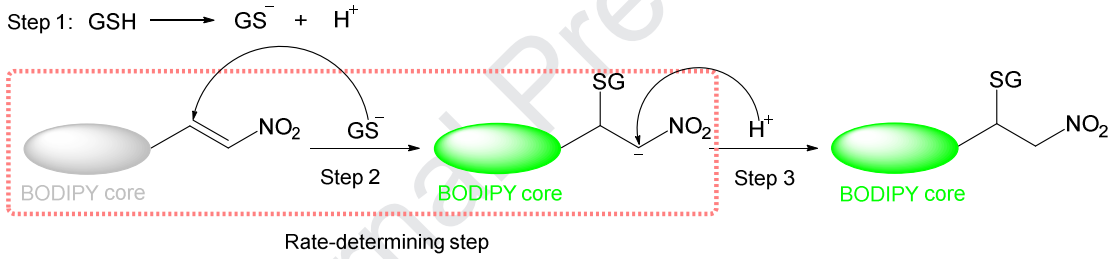

Scheme 4. The speculative reaction mechanism of probes with GSH. Step 1: Thiol deprotonation; Step 2: Conjugate addition; Step 3: Protonation.

We used **BDP-QA** to certify this speculation. First, we detected the final product of **BDP-QA** reacted with GSH in the HEPES buffer (Fig. S40). ^{1}H NMR spectra of **BDP-QA** exhibited protons of olefin double bond at 7.99, 7.96, 7.62 and 7.58 ppm, respectively (Fig. S40a). When reacted with GSH, the protons of olefin double bond disappeared (Fig. S40b). So we speculated that the reaction site should be the olefin double bond. As shown in Fig. S41, we performed the ESI-MS experiment of the reaction solution. After reacting with GSH, the peaks of $[GSH + H]^+$, $[\mathbf{BDP\text{-}QA}]^+$, $[2GSH + H]^+$, $[2GSH + Na]^+$, $[2GSH + K]^+$ and $[\mathbf{BDP\text{-}QA}\text{-}GSH]^+$ appeared in the mass spectrum. Due to the far excess of GSH, the signal corresponding to the adduct was relatively weak. These results proved our speculation of the conjugate addition.

Then, we carried out the kinetic experiments under basic conditions. As shown in Fig. 3, the kinetic experiments were performed at pH 7.4 and 13.0, respectively. It was found that the apparent reaction rate constants were 0.0211 s^{-1} at pH 7.4 and 0.000107 s^{-1} at pH 13.0, respectively. When the pH increased, the rate constant sharply decreased. This might be due to the difficult protonation of the carbanion (Step 3 in Scheme 4) under such a basic condition (pH = 13.0).

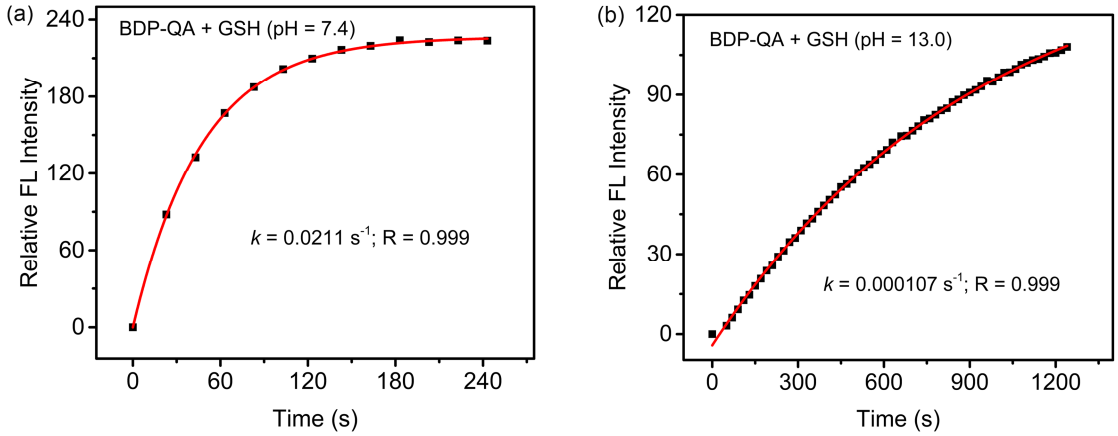

Fig. 3. Kinetics for the reactions of **BDP-QA** with GSH at pH 7.4 (a) and pH 13.0 (b).

With the above results in hand, we considered the effects of hydrophilicity on the reaction rates. Among the four probes, we knew that **BDP-QA** had a positive charge, so we can make a judgment that its hydrophilicity was the largest. Then, we determined the hydrophilicity of other three probes by liquid chromatography mass spectrometry (LC-MS). As shown in Fig. 4, the retention time of **BDP**, **BDP-OEG** and **BDP-OH** were 4.382 min, 2.533 min and 1.550 min, respectively, by extracting extracted ion chromatography (EIC) from total ion chromatography (TIC). Because the chromatographic column of LC-MS apparatus was C-18 reversed-phase column, the sequence of polarity was **BDP-OH** > **BDP-OEG** > **BDP**. The sequence of hydrophilicity would follow this order. So, the hydrophilicity of four probes was in the order of **BDP-QA** > **BDP-OH** > **BDP-OEG** > **BDP**. In combination with the reaction rate constants in Table 2, we could infer that the rate constants were positively correlated with the hydrophilicity of probes.

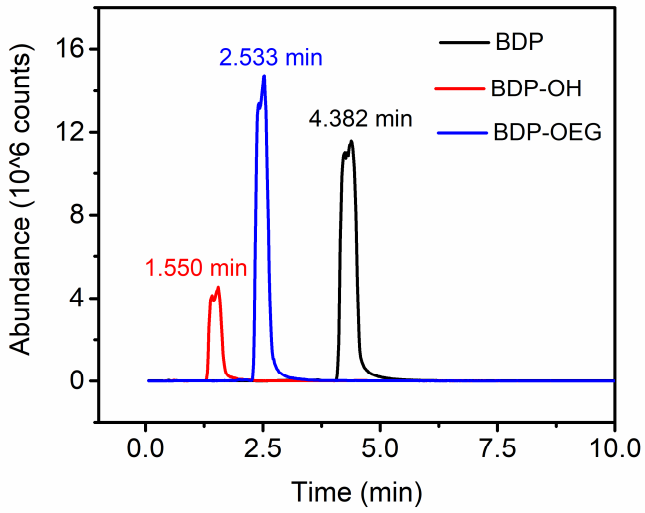

Fig. 4. LC-MS experiments for **BDP**, **BDP-OEG** and **BDP-OH**. The chromatographic column is C-18 reversed-phase column and the eluent is a mixture of acetonitrile and water (*v*/*v* = 8:2).

We further considered whether the ionic strength affected the reaction rate constants in the HEPES buffer. The kinetic experiments were performed under different concentrations of NaCl (Fig. 5a). The ionic strength might influence the quantum yields of fluorescent probes. Though the curves had different final intensities, they would not affect the calculation of rate constants. The curves were fitted with first-order reaction kinetics to obtain the rate constants. As shown in Fig. 5b, as the concentration of NaCl increased (0 ~ 1 M), the rate constant first increased and then slightly decreased. At first, the increased ionic strength would benefit the thiol deprotonation (Step 1 in Scheme 4) by stabilization of thiolate anions, presumably owing to the formation of ion pairs. To be noted, the cationic **BDP-QA** can form ion pairs with the GS^- anion. Exposed to further increased ionic strength, however, it would be harmful to the protonation of the carbanion (Step 3 in Scheme 4) according to the primary salt effect, so the rate constant would decrease. In contrast, the *k* values of other probes increased with the increase of ionic strength (Figs. S42 - 44). This may be due to the favorable stabilization of the thiolate anions (Scheme 4). These

results indicated that the cationic probe had the largest rate constant, possibly owing to the cationic nature of **BDP-QA** and consequently the improved hydrophilicity.

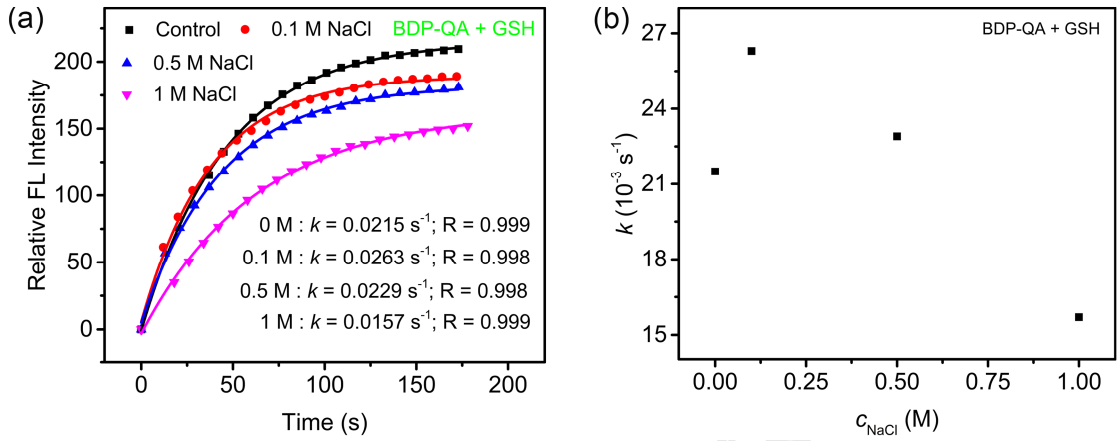

Fig. 5. (a) The kinetic experiments of **BDP-QA** reacted with GSH in the presence of different concentrations of NaCl. (b) Dependence of *k* on the concentration of NaCl for the reaction system of **BDP-QA** and GSH.

To obtain the affinities of the BODIPY-based probes toward GSH, the reaction thermodynamics was further investigated. Owing to the weak fluorescence of probes (the reactants), the enhanced fluorescent intensities can represent the adducts formed by the probes and GSH. The fluorescent intensity is proportional to the concentration of adduct [65]. So, the dependence of fluorescence intensity change (ΔF) on the concentration of reactant (c) can be fitted by eq. (5) [28]:

$$\Delta F = \frac{\mathrm{B}Kc}{(1 + Kc)}$$

where K is the equilibrium constants and B is a constant which has no physical meaning. As shown in Fig 6a, the results indicated that the equilibrium constants gradually decreased with increased temperature. The dependence of equilibrium constant K on the temperature T can be fitted by the van't Hoff equation, eq. (6):

$$lnK = -\frac{\Delta H}{RT} + \frac{\Delta S}{R}$$

where ΔH is the enthalpy change and ΔS is the entropy change. From the linear fitting in Fig. 6b, the enthalpy change and entropy change were - 52.13 kJ mol^{-1} and - 89.79 J mol^{-1} K^{-1}, respectively. The negative ΔS was reasonable since an adduct was formed

by the reaction of **BDP-QA** with GSH. The negative Δ*H* illustrated that the reaction was exothermic. The thermodynamic parameters of other probes with GSH were similar with **BDP-QA** (Figs. S45 - 47). As shown in Table 3, all reactions were exothermic. The more hydrophilicity of probes led to the larger equilibrium constant *K*, *i.e.* the greater affinity. In addition, we calculated the limit of detection (LOD) by eq. (7):

$$\mathrm{LOD} = \frac{3\sigma}{S}$$

where σ is the standard deviation of blank sample values in 10 times, and S is the slope of the linear regression equation. As shown in Table S3, the LOD values for **BDP**, **BDP-OEG**, **BDP-OH** and **BDP-QA** were 14.5 μM, 3.81 μM, 1.55 μM and 182 nM, respectively. We found that the LOD values highly depended on their hydrophilicity. With enhanced water solubility of probes, the LOD values would decrease owing to their better dispersion in water. However, the linearity ranges were gradually narrowed (Table S3).

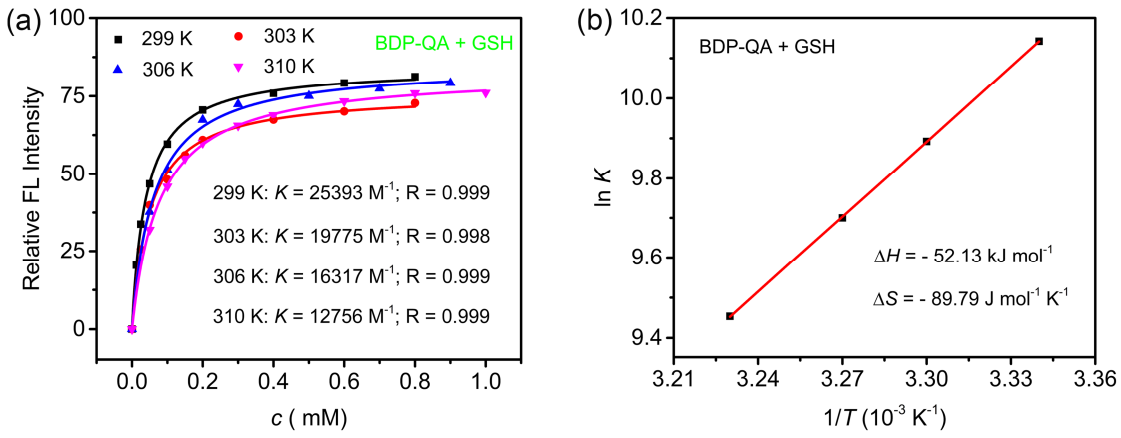

Fig. 6. (a) The reaction of **BDP-QA** with GSH at different temperatures (299 ~ 310 K). (b) Relationship of ln*K* with 1/*T*.

Table 3. The reaction thermodynamic parameters of probes with GSH at ~ 298 K.

	K (M^{-1})	ΔG (kJ mol^{-1})	ΔH (kJ mol^{-1})	ΔS (J mol^{-1} K^{-1})
BDP	1467	- 18.06	- 63.57	- 152.80
BDP-OEG	5268	- 21.23	- 31.69	-34.89
BDP-OH	6681	- 21.82	- 49.15	- 90.54
BDP-QA	25393	- 25.13	- 52.13	- 89.79

4. Conclusions

A series of BODIPY-based probes with different hydrophilic groups, namely **BDP**, **BDP-OEG**, **BDP-OH** and **BDP-QA**, were designed and synthesized. The absorption and fluorescence emission spectra were not affected by these hydrophilic groups. These probes had 27~38 fold fluorescence enhancement in the presence of 10 mM GSH. The cationic **BDP-QA** had the fastest response toward GSH owing to the best water solubility and the possible formation of ion pairs with the thiolate anion. The reaction rate constants of probes were positively correlated with their hydrophilicity. Thermodynamics indicated that the reactions of probes with GSH all had negative ΔH and negative ΔS. The LOD values would be lowered with the increased hydrophilicity. Our work emphasized the importance of hydrophilicity of the fluorescent probes. This work had built the fundamental basis for the design of fluorescent probes with fast response and high affinity.

Acknowledgments

The authors gratefully acknowledge the financial support from National Natural Science Foundation of China (21773178, 21973071, 21573168), the Natural Science Foundation of Hubei Province (2018CFA090), Guangxi Science and Technology Project (GuiKeAD17195081), and Bagui Scholar Program of Guangxi Province (2016).

References

[1] Wang Q, Wang H, Huang J, Li N, Gu Y, Wang P. Novel NIR fluorescent probe with dual models for sensitively and selectively monitoring and imaging Cys in living cells and mice. Sensor Actuat B Chem 2017;253:400-6.

[2] Zhang J, Jiang XD, Shao X, Zhao J, Su Y, Xi D, et al. A turn-on NIR fluorescent probe for the detection of homocysteine over cysteine. RSC Adv 2014;4(96):54080-3.

[3] Tang B, Xing YL, Li P, Zhang N, Yu FB, Yang GW. A rhodamine-based fluorescent probe containing a Se-N bond for detecting thiols and its application in living cells. J Am Chem Soc 2007;129:11666-7.

[4] Isik M, Ozdemir T, Turan IS, Kolemen S, Akkaya EU. Chromogenic and fluorogenic sensing of biological thiols in aqueous solutions using BODIPY-based reagents. Org Lett 2013;15(1):216-9.

[5] Chen WQ, Luo HC, Liu XJ, W. Foley J, Song XZ. Broadly applicable strategy for the fluorescence based detection and differentiation of glutathione and cysteine/homocysteine. Anal Chem 2016;88(7):3638-46.

[6] Pacsial-Ong EJ, L.McCarley R, Wang WH, M. Strongin R. Electrochemical detection of glutathione using redox indicators. Anal Chem 2006;78(21):7577-81.

[7] Ferin R, Pavão ML, Baptista J. Methodology for a rapid and simultaneous determination of total cysteine, homocysteine, cysteinylglycine and glutathione in plasma by isocratic RP-HPLC. J Chromatogr B 2012;911:15-20.

[8] Calvo-Marzal P, Chumbimuni-Torres KY, Hoehr NF, Kubota LT. Determination of glutathione in hemolysed erythrocyte with amperometric sensor based on TTF-TCNQ. Clin Chim Acta 2006;371(1-2):152-8.

[9] Niu LY, Jia MY, Chen PZ, Chen YZ, Zhang Y, Wu LZ, et al. Colorimetric sensors with different reactivity for the quantitative determination of cysteine, homocysteine and glutathione in a mixture. RSC Adv 2015;5:13042-5.

[10] Lee S, Li J, Zhou X, Yin J, Yoon J. Recent progress on the development of glutathione (GSH) selective fluorescent and colorimetric probes. Coordin Chem Rev 2018;366:29-68.

[11] Chen J, Wang Z, She M, Liu M, Zhao Z, Chen X. Precise synthesis of GSH-specific fluorescent probe for hepatotoxicity assessment guided by theoretical calculation. ACS Appl Mater Interfaces 2019;11 (36):32605-12.

[12] Umezawa K, Yoshida M, Kamiya M, Yamasoba T, Urano Y. Rational design of reversible fluorescent probes for live-cell imaging and quantification of fast glutathione dynamics. Nat Chem 2017;9(3):279-86.

[13] Yin CX, Xiong KM, Huo FJ, Salamanca JC, Strongin RM. Fluorescent probes with multiple binding sites for the discrimination of Cys, Hcy, and GSH. Angew Chem Int Ed 2017;56(43):13188-98.

[14] Bao G, Wong KL, Tanner PA. A reversible rhodamine B based pH probe with large pseudo-stokes shift. ChemPlusChem 2019;84:816-20.

[15] Tian M, He H, Wang BB, Wang X, Liu Y, Jiang FL. A reaction-based turn-on fluorescent sensor for the detection of Cu (II) with excellent sensitivity and selectivity: synthesis, DFT calculations, kinetics and application in real water samples. Dyes Pigments 2019;165:383-90.

[16] Huang R, Wang BB, Si-Tu XM, Gao T, Jiang FL, Liu Y, et al. A lysosome-targeted fluorescent sensor for the detection of glutathione in cells with an extremely fast response. Chem Commun 2016;52:11579-82.

[17] Tian M, Yang M, Liu Y, Jiang FL. Rapid and reversible reaction-based ratiometric fluorescent probe for imaging of different glutathione levels in living cells. ACS Appl Bio Mater 2019;2(10):4503-14.

[18] Cheng T, Huang W, Gao D, Yang Z, Zhang C, Zhang H, et al. Michael addition/S, N-intramolecular rearrangement sequence enables selective fluorescence detection of cysteine and homocysteine. Anal Chem 2019;91(16):10894-900.

[19] Jiang X, Yu Y, Chen J, Zhao M, Chen H, Song X, et al. Quantitative imaging of glutathione in live cells using a reversible reaction-based ratiometric fluorescent probe. ACS Chem Biol 2015;10(3):864-74.

[20] Jiang XQ, Chen JW, Bajić A, Zhang CW, Song XZ, L. Carroll S, et al. Quantitative real-time imaging of glutathione. Nat Commun 2017;8:16087.

[21] Zhang X, He N, Huang Y, Yu F, Li B, Lv CJ, et al. Mitochondria-targeting near-infrared ratiometric fluorescent probe for selective imaging of cysteine in orthotopic lung cancer mice. Sensor Actuat B Chem 2019;282:69-77.

[22] Xu Z, Zhang MX, Xu Y, Liu SH, Zeng L, Chen H, et al. The visualization of lysosomal and mitochondrial glutathione via near-infrared fluorophore and in vivo imaging application. Sensor Actuat B Chem 2019;290:676-83.

[23] Zhang M, Wu YC, Zhang SZ, Zhu HN, Wu Q, Jiao LJ, Hao EH. A nitroolefin functionalized BODIPY chemodosimeter for biothiols driven by an unexpected conjugated addition mechanism. Chem Commun 2012;48:8925-7.

[24] Gao T, He H, Huang R, Wang FF, Hu YJ, Jiang FL, et al. BODIPY-based fluorescent probes for mitochondria-targeted cell imaging with superior brightness, low cytotoxicity and high photostability. Dyes Pigments 2017;141:530-5.

[25] Lv F, Tang B, Hao E, Liu QY, Wang H, Jiao L. Transition-metal-free regioselective cross-coupling of BODIPYs with thiols. Chem Commun 2019;55(11):1639-42.

[26] Lincoln R, Greene LE, Zhang W, Louisia S, Cosa G. Mitochondria alkylation and cellular trafficking mapped with a lipophilic BODIPY-acrolein fluorogenic probe. J Am Chem Soc 2017;139(45):16273-81.

[27] Huang L, Duan R, Li Z, Zhang Y, Zhao J, Han G. BODIPY-based nanomicelles as near-infrared fluorescent “Turn-On” sensors for biogenic thiols. Chem Nano Mater 2016;2(5):396-9.

[28] Wang FF, Fan XY, Liu YJ, Gao T, Huang R, Jiang FL, et al. Design, synthesis, cell imaging, kinetics and thermodynamics of reaction-based turn-on fluorescent probes for the detection of biothiols. Dyes Pigments 2017;145:451-60.

[29] Lu H, Mack J, Yang Y, Shen Z. Structural modification strategies for the rational design of red/NIR region BODIPYs. Chem Soc Rev 2014;43(13):4778-823.

[30] Kand D, Liu P, X. Navarro M, J. Fischer L, W. Miller E, Weinstain R, et al. Water-soluble BODIPY photocages with tunable cellular localization. J Am Chem Soc

2020;142:4970-4.

[31] Wang FF, Liu YJ, Wang BB, Gao LX, Jiang FL and Liu Y. A BODIPY-based mitochondria-targeted turn-on fluorescent probe with dual response units for the rapid detection of intracellular biothiols. Dyes Pigments 2018;152:29-35.

[32] Nierth A, Yu. Kobitski A, Nienhaus GU, Jäschke A. Anthracene-BODIPY dyads as fluorescent sensors for biocatalytic Diels-Alder reactions. J Am Chem Soc 2010;132:2646-54.

[33] Yao HW, Zhu XY, Guo XF, Wang H. An amphiphilic fluorescent probe designed for extracellular visualization of nitric oxide released from living cells. Anal Chem 2016;88(18):9014-21.

[34] Zhang J, Bao X, Zhou J, Peng F, Ren H, Dong X, et al. A mitochondria-targeted turn-on fluorescent probe for the detection of glutathione in living cells. Biosens Bioelectron 2016;85:164-70.

[35] Zhu H, Fan J, Mu H, Zhu T, Zhang Z, Du J, et al. D-PET-controlled “off-on” polarity-sensitive probes for reporting local hydrophilicity within lysosomes. Sci Rep 2016;6:35627.

[36] Atilgan S, Ekmekci Z, Dogan AL, Guc D, Akkaya EU. Water soluble distyryl-boradiazaindacenes as efficient photosensitizers for photodynamic therapy. Chem Commun 2006;(42):4398-400

[37] Turan IS, Cakmak FP, Yildirim DC, Cetin-Atalay R, Akkaya EU. Near-IR absorbing BODIPY derivatives as glutathione-activated photosensitizers for selective photodynamic action. Chem Eur J 2014;20:16088-92.

[38] Niu LY, Guan YS, Chen YZ, Wu LZ, Tung CH, Yang QZ. BODIPY-based ratiometric fluorescent sensor for highly selective detection of glutathione over cysteine/homocysteine. J Am Chem Soc 2012;134(46):18928-31.

[39] Vegesna GK, Sripathi SR, Zhang J, Zhu S, He W, Luo FT, et al. Highly water-soluble BODIPY-based fluorescent probe for sensitive and selective detection of nitric oxide in living cells. ACS Appl Mater Interfaces 2013;5(10):4107-12.

[40] Niko J. Meltola RW, Aleksi E. Soini. Hydrophilic labeling reagents of dipyrrylmethene-BF_2 dyes for two-photon excited fluorometry: syntheses and photophysical characterization. J Fluoresc 2004;14:635-47.

[41] Wang P, Na ZK, Fu JQ, Y. J. Tan C, Zhang HT, Q. Yao S, et al. Microarray immobilization of biomolecules using a fast trans-cyclooctene (TCO)-teraine reaction. Chem Commun 2014;50:11818-21.

[42] Worsfold O, H. Voelcker N, Nishiya T. Biosensing using lipid bilayers suspended on porous silicon. Langmuir 2006;22:7078-83.

[43] Tan Y, Cheng YX, Zhang SY, Zhu WP, Qian XH, Duan LP. A highly sensitive and selective OFF-ON fluorescent sensor for cadmium in aqueous solution and living cell. J Am Chem Soc 2008;130:16160-1.

[44] C. Dodani S, He QW, J. Chang C. A turn-on fluorescent sensor for detecting nickel in living cells. J Am Chem Soc 2009;131:18020-1.

[45] Wang C, Song X, Chen L, Xiao Y. Specifically and wash-free labeling of SNAP-tag fused proteins with a hybrid sensor to monitor local micro-viscosity. Biosens Bioelectron 2017;91:313-20.

[46] Fan J, Han Z, Kang Y, Peng X. A two-photon fluorescent probe for lysosomal thiols in live cells and tissues. Sci Rep 2016;6:19562.

[47] Yin J, Kwon Y, Kim D, Lee D, Kim G, Hu Y, et al. Cyanine-based fluorescent probe for highly selective detection of glutathione in cell cultures and live mouse tissues. J Am Chem Soc 2014;136(14):5351-8.

[48] Zhang Q, Ding S, Zhai Q, Feng G. Highly sensitive and selective detection of biothiols by a new low dose colorimetric and fluorescent probe. RSC Adv 2015;5(77):62325-30.

[49] Xie X, Li M, Tang F, Li Y, Zhang L, Jiao X, et al. Combinatorial strategy to identify fluorescent probes for biothiol and thiophenol based on diversified pyrimidine moieties and their biological applications. Anal Chem 2017;89(5):3015-20.

[50] Zhu B, Zhang X, Li Y, Wang P, Zhang H, Zhuang X. A colorimetric and ratiometric fluorescent probe for thiols and its bioimaging applications. Chem Commun 2010;46(31):5710-2.

[51] Lim CS, Masanta G, Kim HJ, Han JH, Kim HM, Cho BR. Ratiometric detection of mitochondrial thiols with a two-photon fluorescent probe. J Am Chem Soc 2011;133(29):11132-5.

[52] Kim GJ, Lee K, Kwon H, Kim HJ. Ratiometric fluorescence imaging of cellular glutathione. Org Lett 2011;13: 2799-801.

[53] Pang L, Zhou Y, Wang E, Yu F, Zhou H, Gao W. A “turn-on” fluorescent probe used for the specific recognition of intracellular GSH and its application in bioimaging. RSC Adv 2016;6(20):16467-73.

[54] Yang XY, Guo YX, M. Strongin R. Conjugate addition/cyclization sequence enables selective and simultaneous fluorescence detection of cysteine and homocysteine. Angew Chem Int Ed 2011;50:10690-3.

[55] Lim SJ; O. Escobedo J, Lowry M, Xu XY, Strongin R. Selective fluorescence detection of cysteine and N-terminal cysteine peptide residues. Chem Commun 2010;46:5707-5709.

[56] Hong V, A. Kislukhin A, Finn MG. Thiol-selective fluorogenic probes for labeling and release. J Am Chem Soc 2009;131:9986-94.

[57] Ros-Lis JV, Garcia B, Jimenez D, Martınez-Manez R, Sancenon F, Soto J, et al. Squaraines as fluoro-chromogenic probes for thiol-containing compounds and their application to the detection of biorelevant thiols. J Am Chem Soc 2004;126:4064-5.

[58] Guo Z, Nam S, Park S, Yoon J. A highly selective ratiometric near-infrared fluorescent cyanine sensor for cysteine with remarkable shift and its application in bioimaging. Chem Sci 2012;3:2760-5.

[59] Sun YQ, Chen M, Liu J, Lv X, Li JF, Guo W. Nitroolefin-based coumarin as a colorimetric and fluorescent dual probe for biothiols. Chem Commun 2011;47:11029-31.

[60] Zhang M, Wu Y, Zhang S, Zhu H, Wu Q, Jiao L, et al. A nitroolefin functionalized BODIPY chemodosimeter for biothiols driven by an unexpected conjugated addition mechanism. Chem Commun 2012;48:8925-7.

[61] Isik M, Guliyev R, Kolemen S, Altay Y, Senturk B, Tekinay T, et al. Designing an intracellular fluorescent probe for glutathione: two modulation sites for selective signal transduction. Org Lett 2014;16(12):3260-3.

[62] Chen JW, Jiang XQ, L. Carroll S, Huang J and Wang J. Theoretical and experimental investigation of thermodynamics and kinetics of thiol-michael addition reactions: A case study of reversible fluorescent probes for glutathione imaging in single cells. Org Lett 2015;17:5978-81.

[63] H. Krenske E, C. Petter R, Zhu ZD and N. Houk K. Transition states and energetics of nucleophilic additions of thiols to substituted α,β-unsaturated ketones: substituent effects involve enone stabilization, product branching, and solvation. J Org Chem 2011;76:5074-81.

[64] Mayer RJ, Ofial AR. Nucleophilicity of glutathione: a link to Michael acceptor reactivities. Angew. Chem. Int. Ed. 2019;58:17704-8.

[65] Skoog DA, West DM, Holler FJ, Crouch SR. Fundamentals of analytical chemistry: Nelson education. 2013.

Highlight:

(1) OFF-ON fluorescent detection based on the conjugate addition with nitroolefin.

(2) The greater hydrophilicity, the faster response.

(3) The fastest response, highest affinity and lowest LOD with cationic **BDP-QA**.

Declaration of interests

☒ The authors declare that they have no known competing financial interests or personal relationships that could have appeared to influence the work reported in this paper.

☐The authors declare the following financial interests/personal relationships which may be considered as potential competing interests: